https://doi.org/10.5194/egusphere-2026-3511
Preprint. Discussion started: 29 June 2026

Southern Ocean dominance and basin asymmetry in centennial-scale bottom-water return

Guangchuang Zhang[1], Zhongya Cai[2,3], Zhiqiang Liu[1,4]

[1]Department of Ocean Science and Engineering, Southern University of Science and Technology, Shenzhen, China
[2]State Key Laboratory of Internet of Things for Smart City, and Department of Ocean Science and Technology, University of Macau, Macau, China
[3]Center for Ocean Research in Hong Kong and Macau (CORE), Hong Kong
[4]Center for Complex Flows and Soft Matter Research, Southern University of Science and Technology, Shenzhen, China

Correspondence to: Zhiqiang Liu (liuzq@sustech.edu.cn)

Abstract. Return of abyssal bottom waters toward the upper ocean is a key component of overturning closure because it reconnects the deep ocean with surface-influenced layers and helps regulate the redistribution of heat, carbon, and nutrients. Yet the large-scale organization and timing of this return remain incompletely quantified. Here we combine the 1/12° GLORYS12 global ocean reanalysis with Constituent-oriented Age and Residence time Theory to diagnose bottom-water concentration, ventilation thickness, concentration-weighted diapycnal transport, and water age within a single framework. The results reveal a globally connected but strongly basin-asymmetric return structure. The Southern Ocean forms the dominant return hub, where strong cross-isopycnal exchange and broad outcropping pathways provide the principal route through which abyssal waters reach lighter, upper-ocean-connected density classes within the centennial diagnostic window. Beyond this circumpolar branch, the Atlantic exhibits broad and comparatively efficient upward penetration, the Pacific retains older bottom waters and weaker ascent through much of the basin, and the Indian Ocean displays more spatially focused subtropical and ridge-associated return corridors. These results show that abyssal return is not a single diffuse background upwelling branch, but a basin-dependent structure shaped by Southern Ocean upwelling, topographic mixing, equatorial exchange, and basin-scale overturning geometry. Together, the diagnostics provide a global view of where bottom-water influence rises, how strongly it fills the water column, and how renewal timescales differ among basins.

1 Introduction

The global Meridional Overturning Circulation (MOC) links surface, deep, and abyssal waters through coupled upper and lower overturning cells and plays a central role in climate regulation and biogeochemical cycling (Cessi, 2019; Lee et al., 2019, 2023; Lumpkin and Speer, 2007; Marshall and Speer, 2012). In the lower cell, dense waters formed at high latitudes must ultimately leave the abyss, cross neutral-density classes, and reconnect with the upper ocean through a combination of diapycnal exchange, isopycnal spreading, and Southern Ocean outcropping (Cimoli et al., 2023; Ferrari, 2014; Ferrari et al., 2017; Talley, 2013). How and where this abyssal return occurs helps set the redistribution of heat, carbon, oxygen, and

https://doi.org/10.5194/egusphere-2026-3511
Preprint. Discussion started: 29 June 2026

nutrients over decadal to centennial timescales and therefore influences how the deep ocean communicates with the climate system.

By contrast with upper-ocean ventilation, which has been extensively examined using tracer, water-mass, and circulation diagnostics (Blanke et al., 2002; England, 1995; Liu and Tanhua, 2024; Morrison et al., 2022), the return of abyssal bottom waters to the upper ocean remains more difficult to resolve because it involves several linked processes: dense-water formation and abyssal spreading, transformation across density surfaces, and subsequent along-isopycnal export toward regions where density surfaces outcrop. Classical views often invoked broad, weak, and nearly uniform deep upwelling to close the overturning circulation (Munk, 1966; Stommel and Arons, 1959). Subsequent work has instead reframed abyssal return as a spatially heterogeneous and mechanism-dependent process. The principal mechanisms include Southern Ocean wind-driven upwelling and isopycnal outcropping, topographically enhanced turbulent mixing over ridges, slopes, and canyons, near-boundary mixing layers that can drive thin upslope upwelling, and internal-wave or geothermal water-mass transformation that consumes or modifies Antarctic Bottom Water (AABW) within abyssal basins (De Lavergne et al., 2016, 2017; Marshall and Speer, 2012; McDougall and Ferrari, 2017; Nikurashin and Ferrari, 2013). These processes imply that abyssal bottom-water return is organized around preferential dynamical pathways rather than a single diffuse background upwelling field, as summarized schematically in Fig. 1.

Observational and modeling studies have constrained several parts of this mechanism chain. Microstructure compilations and tracer-release experiments show that abyssal mixing is strongly enhanced over rough topography and near abrupt ridges, where internal waves break and drive water-mass transformation (Ledwell et al., 2000; Waterhouse et al., 2014). Recent studies further demonstrate that mixing in boundary layers, submarine canyons, and topographically rough Southern Ocean can focus AABW upwelling into narrow but dynamically important regions (Baker et al., 2023; Holmes et al., 2019; McDougall and Ferrari, 2017; Wynne-Cattanach et al., 2024). At larger scales, the distribution of seafloor roughness and internal-wave dissipation helps shape the abyssal overturning geometry and the removal of dense waters from abyssal basins (De Lavergne et al., 2016, 2017; Nikurashin and Ferrari, 2013), while Pacific studies emphasize that tidal mixing away from the seafloor and equatorial/inter-basin pathways can influence deep ventilation far from the primary Southern Ocean source regions (Oka and Niwa, 2013; Shah et al., 2017).

These studies clarified key regional mechanisms, but a global, basin-comparative diagnosis of where bottom-water influence spreads most efficiently, how strongly it fills the water column, and how rapidly it returns is still limited. A further difficulty is that no single diagnostic captures the full structure of abyssal return. Cross-isopycnal velocity identifies where vertical exchange is dynamically active, whereas tracer concentration reveals where bottom-water influence propagates. A coherent physical interpretation therefore requires these diagnostics to be examined together, so that pathway geometry, vertical extent, and transport intensity can be assessed within one global framework.

https://doi.org/10.5194/egusphere-2026-3511
Preprint. Discussion started: 29 June 2026

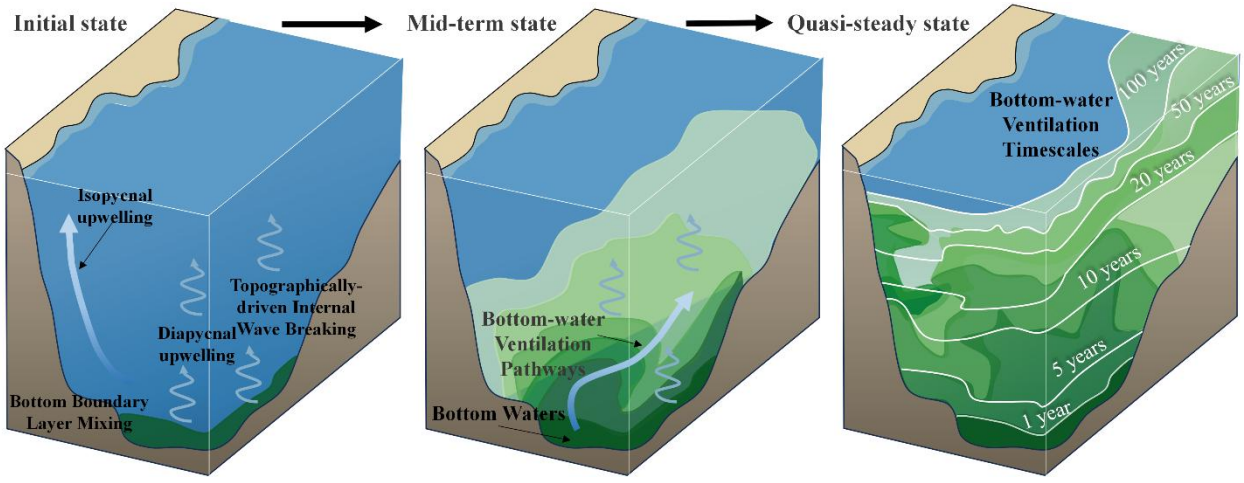

Figure 1 Conceptual schematic of global bottom-water upward ventilation. In the initial state, dense bottom waters occupy abyssal layers. Topographically enhanced internal-wave breaking and bottom-boundary-layer mixing induce diapycnal mixing and cross-isopycnal exchange, allowing bottom waters to enter lighter density classes. In the intermediate state, transformed bottom-water signals propagate upward and laterally along ventilation pathways following their emergence into the ocean interior. In the quasi-steady state, bottom-water influence extends throughout the ocean interior and exhibits increasing ventilation water age with distance from source and transformation regions. The schematic summarizes the coupled roles of diapycnal transformation, pathway geometry, and renewal timescales in shaping the abyssal bottom-water return.

Another key issue is the timescale of bottom-water return, which provides the temporal counterpart to pathway diagnostics, as illustrated schematically in Fig. 1. Ventilation water age diagnoses the mean elapsed time since a water parcel last contacted the bottom layer, and is therefore essential for distinguishing rapidly renewed return corridors from slowly ventilated abyssal reservoirs (England, 1995; Fine et al., 2017; Waugh et al., 2003). Observations and models show that AABW ventilation can vary substantially among Southern Ocean sectors and abyssal basins, while recent changes in formation, freshening, oxygen supply, and meltwater forcing are altering abyssal renewal and aging on decadal to centennial timescales (Gunn et al., 2023; Li et al., 2023; Purkey et al., 2018; Shimada et al., 2022). In addition, Tamsitt et al. (2017) showed that deep waters can follow spiraling ascent pathways into the Southern Ocean surface over multidecadal timescales. These findings motivate our use of water age as a diagnostic for evaluating the renewal timescale of bottom-water return within a global framework.

Here we combine the high-resolution (1/12°) GLORYS12 global ocean reanalysis with Constituent-oriented Age and Residence time Theory (CART) to diagnose bottom-water return using four complementary metrics: bottom-water concentration, ventilation thickness, concentration-weighted diapycnal transport, and water age. Our aim is to identify the dominant regions through which abyssal waters return, quantify the major Atlantic-Pacific-Indian contrasts in pathway structure and timing, and interpret those contrasts in the context of Southern Ocean upwelling, topographic mixing, and basin-scale overturning geometry. This approach yields a global diagnostic picture of how bottom-water pathways and renewal timescales differ among basins and which regions serve as the principal gateways through which abyssal waters reconnect with the upper ocean.

https://doi.org/10.5194/egusphere-2026-3511
Preprint. Discussion started: 29 June 2026

2 Data and methods

2.1 Constituent-oriented Age and Residence time Theory

We use the GLORYS12 global ocean reanalysis from the Copernicus Marine Environment Monitoring Service (CMEMS) to diagnose bottom-water return pathways and timescales. GLORYS12 has a nominal horizontal resolution of 1/12°, 50 vertical levels, and coverage from 1993 to the present (Jean-Michel et al., 2021; Lellouche et al., 2018). Its eddy-rich circulation and dynamically consistent hydrographic structure make it well suited for tracing large-scale abyssal return and for comparing how that return differs among basins (Artana et al., 2021; Du Pontavice et al., 2023; Verezemskaya et al., 2021).

To quantify bottom-water return, we apply CART to two complementary tracers: bottom-water-origin concentration (C) and its associated age concentration (Γ) (Deleersnijder et al., 2001; Delhez, 2006; Delhez et al., 1999). The diagnosed concentration represents the fraction of water at a given location that originates from the model bottom layer. This tracer identifies the spatial imprint of bottom-water influence and is used to examine bottom-water pathways in Sect. 3.2. The ratio of age concentration to concentration, referred to as water age ($A = \Gamma/C$), represents the mean elapsed time since contact with the bottom layer and is used to quantify the renewal timescale of bottom-water influence in Sect. 3.3.

The governing equations for these two tracers are:

$$\frac{\partial C}{\partial t} + \nabla \cdot (\boldsymbol{u}C) = \frac{\partial}{\partial z}\left(K_T \frac{\partial C}{\partial z}\right) \quad (1)$$

$$\frac{\partial \Gamma}{\partial t} + \nabla \cdot (\boldsymbol{u}\Gamma) = \frac{\partial}{\partial z}\left(K_T \frac{\partial \Gamma}{\partial z}\right) + C \quad (2)$$

where $\boldsymbol{u}$ is the three-dimensional velocity field from GLORYS12, z is the vertical layer depth, and K_T is the eddy-diffusivity tensor estimated with the K-profile parameterization scheme (Large et al., 1994). The first equation describes the advection and diffusion of bottom-water-origin concentration, and the second applies the same transport operator to the associated age concentration so that water age can be diagnosed consistently within the same framework.

All CART calculations were performed under monthly climatological forcing derived from GLORYS12, and the simulation was integrated for 100 years. We analyze annual-mean concentration and water age fields from this centennial integration. A concentration threshold of 0.05 is used to identify regions effectively reached by bottom-water signals, and a concentration-tendency threshold ($\partial C/\partial t$) of 10^{-3} is used to identify locations that have approached quasi-equilibrium. These criteria focus the analysis on the large-scale pathway and renewal-time structure resolved within the diagnostic window.

To evaluate the sensitivity of the quasi-equilibrium criterion, we compared the global equilibrium times diagnosed using the baseline concentration-tendency threshold of 10^{-3} with those diagnosed using alternative thresholds of 10^{-4} and 10^{-2} (Supplementary Fig. S1). This comparison was performed as two separate binned scatter analyses. The results show that the more stringent threshold of 10^{-4} generally yields longer equilibrium times, whereas the less stringent threshold of 10^{-2} yields shorter equilibrium times. Nevertheless, the binned distributions and weighted-median fits show that the relative spatial structure of the diagnosed equilibrium times remains largely consistent across threshold choices, with R^2 values of 0.88 for

https://doi.org/10.5194/egusphere-2026-3511
Preprint. Discussion started: 29 June 2026

10^{-4} and 0.90 for 10^{-2}. This indicates that the large-scale pathway geometry and associated renewal-timescale structure are not strongly affected by the specific threshold selected. The baseline threshold of 10^{-3} therefore provides a practical balance between identifying the dominant ventilation pathways and limiting the influence of the slow residual tail associated with weak background diffusion.

Taken together, the concentration, water age, ventilation thickness, and concentration-weighted cross-isopycnal flux diagnostics identify where bottom waters return, how strongly they influence different regions, and on what timescales that return occurs. Interpreting these complementary fields jointly allows pathway geometry, vertical extent, transport intensity, and renewal timescale to be evaluated within a single global analysis.

2.2 Diapycnal velocity

Building on the CART framework described above, the diapycnal velocity diagnostic provides the dynamical link between the tracer-based measures of bottom-water influence and the physical transformation required for abyssal return. The concentration, water age, ventilation thickness, and concentration-weighted diapycnal flux diagnostics identify where bottom-water signals extend, how strongly they affect the water column, and on what timescales they return. The physical reconnection of bottom waters with the upper ocean occurs through cross-isopycnal transformation into lighter density classes (Ferrari, 2014; Lumpkin and Speer, 2007; Marshall and Speer, 2012; Talley, 2013). This transformation is enabled by diapycnal exchange driven by diapycnal mixing, a process known to be highly heterogeneous in space, with enhanced mixing occurring preferentially near rough topography, boundaries, and dynamically active Southern Ocean regions (Cimoli et al., 2023; Ledwell et al., 2000; Ruan and Ferrari, 2021; Wynne-Cattanach et al., 2024). We therefore diagnose the diapycnal velocity, which represents the rate of water motion across moving density surfaces, to identify where cross-density exchange most effectively supports bottom-water return (Bennett, 1986; Ferrari et al., 2016; Marshall et al., 1999).

Following Ferrari et al. (2016), the diagnosed diapycnal velocity is defined relative to moving isopycnal surfaces rather than as the Eulerian velocity projected onto a fixed isopycnal surface normal. This distinction is important because density surfaces themselves migrate in time, so apparent motion normal to a fixed surface does not necessarily represent true exchange across density classes. The diapycnal velocity ω_d is defined as the difference between the Eulerian velocity component normal to the isopycnal surface ($\boldsymbol{u} \cdot \boldsymbol{n}_\rho$) and the velocity of an isopycnal surface in the direction normal to itself ($\boldsymbol{u_\rho}$) ,

$$\omega_d = (\boldsymbol{u} \cdot \boldsymbol{n}_\rho)\boldsymbol{n}_\rho - \boldsymbol{u}_\rho, \tag{3}$$

where $\boldsymbol{u}$ is the three-dimensional velocity field and $\boldsymbol{n}_\rho = \nabla\gamma^n/|\nabla\gamma^n|$ is the unit normal vector to the isopycnal surface. The velocity of the moving density surface, $\boldsymbol{u}_\rho$, is estimated following Marshall et al. (1999) as

$$\boldsymbol{u}_\rho = -\frac{1}{|\nabla\gamma^n|}\frac{\partial\gamma^n}{\partial t}\boldsymbol{n}_\rho, \tag{4}$$

https://doi.org/10.5194/egusphere-2026-3511
Preprint. Discussion started: 29 June 2026

where γ^n is the neutral density from GLORYS12. Neutral density provides a dynamically consistent framework for tracing large-scale water-mass pathways (Jackett and Mcdougall, 1997; Orsi et al., 1999), and its zonal-mean structure for the global ocean and individual basins is shown in Supplementary Fig. S3.

The diagnosed diapycnal velocity isolates exchange across density classes and is therefore used here as a dynamical indicator of where bottom-water transformation and upward return are most actively supported within the global overturning circulation. It also provides the dynamical basis for the concentration-weighted diapycnal flux diagnostic introduced in Sect. 3.2, which links cross-isopycnal transport to the distribution of bottom-water influence.

3 Results

To resolve abyssal return as a connected physical problem, we examine a sequence of diagnostics that capture complementary aspects of the same process. We first diagnose the density-space and horizontal structure of diapycnal motion, because bottom-water return requires cross-isopycnal exchange (Sect. 3.1). We then combine ventilation thickness, concentration distribution, and concentration-weighted diapycnal flux to characterize where bottom-water signals accumulate, how they spread into lighter density classes, and where upward transformation is most effective (Sect. 3.2). Finally, we use water age to constrain the timescales over which these pathways operate (Sect. 3.3). Viewed together, these diagnostics provide a coherent picture of where abyssal return occurs, how it differs among basins, and how rapidly it reconnects bottom waters with the upper ocean.

3.1 Global Ocean Diapycnal Motion

As defined in Sect. 2.2, the diagnosed diapycnal velocity represents the rate of water motion across moving isopycnal surfaces (Bennett, 1986; Ferrari et al., 2016; Marshall et al., 1999). It therefore serves as the most direct dynamical diagnostic of global ocean diapycnal motion, revealing where cross-isopycnal exchange is dynamically active and thus where abyssal return is physically enabled.

To examine the horizontal structure of abyssal cross-isopycnal exchange, diapycnal velocity is shown on the neutral-density surface $\gamma^n = 28.1$ kg m^{-3} (roughly 3000 m; Supplementary Fig. S3) in Fig. 2a. This density surface lies near the transition between the abyssal bottom-water domain and the overlying deep water and therefore provides a useful reference surface for diagnosing where bottom-water transformation is most active. The map reveals alternating upwelling and downwelling patches across all major basins, confirming that abyssal return is not organized as a spatially uniform background process. Instead, the strongest upward signals are concentrated in geographically localized regions.

https://doi.org/10.5194/egusphere-2026-3511
Preprint. Discussion started: 29 June 2026

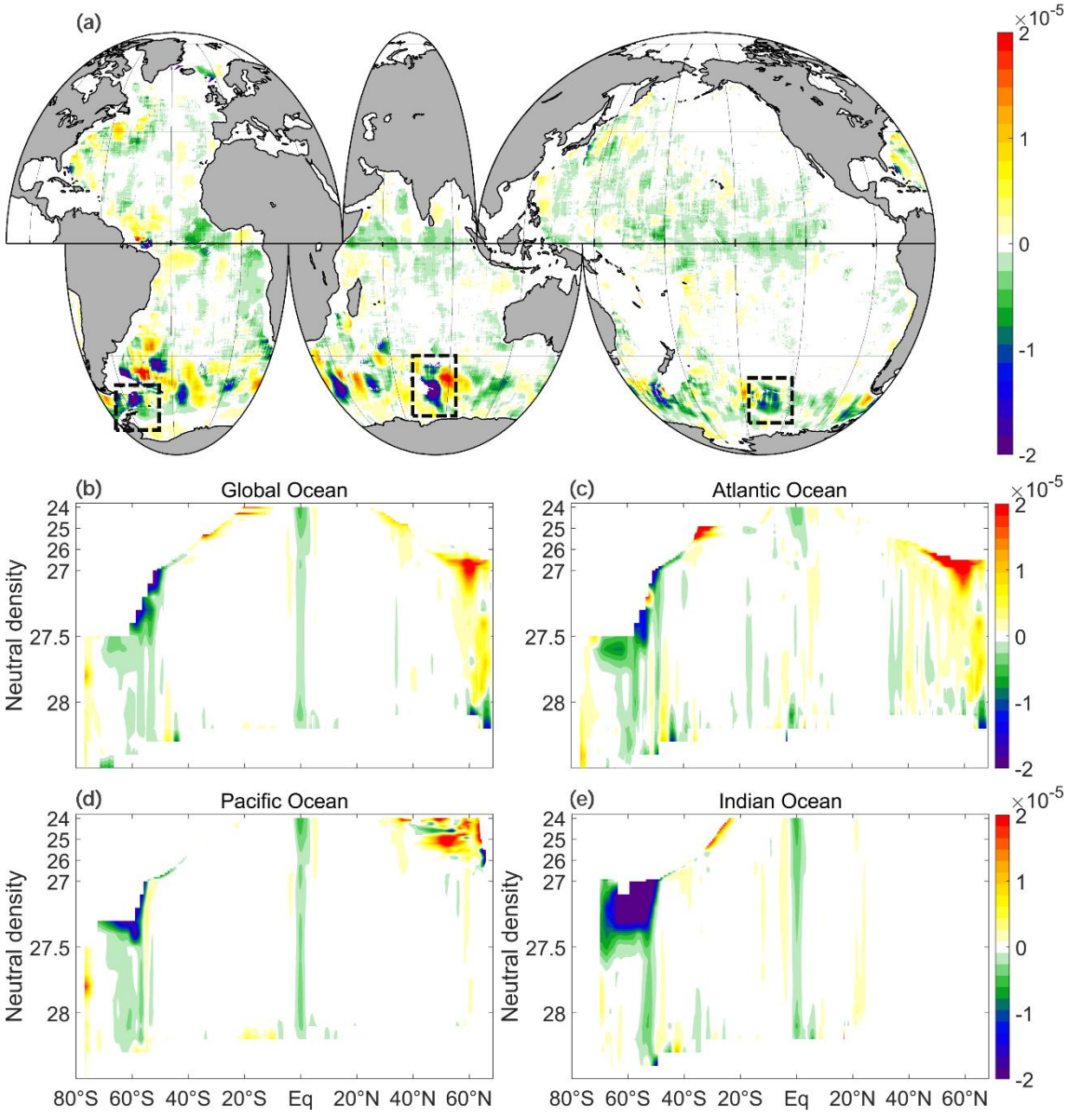

Figure 2 Diapycnal velocity ($\mathrm{m\,s^{-1}}$) as a diagnostic of global ocean diapycnal motion. (a) Global distribution of diapycnal velocity on the neutral-density surface $\gamma^n = 28.1\,\mathrm{kg\,m^{-3}}$, where positive values indicate transport toward denser classes (downwelling) and negative values indicate transport toward lighter classes (upwelling). Black dashed boxes mark representative Southern Ocean hotspots of intensified diapycnal upwelling associated with major topographic features, including Drake Passage, the Kerguelen Plateau, and the Campbell Plateau. The corresponding global bathymetry is shown in Supplementary Fig. S4. (b–e) Zonal-mean distributions of the 30-year mean diapycnal velocity in the global ocean, Atlantic Ocean, Pacific Ocean, and Indian Ocean. Together, these panels illustrate the large-scale spatial organization of cross-isopycnal exchange in the global overturning circulation.

The most prominent upwelling hotspots occur in the Southern Ocean, the equatorial Pacific, and selected deep western boundary regions. In the Southern Ocean, enhanced upward motion is closely associated with major topographic regions, including Drake Passage, the Kerguelen Plateau, and the Campbell Plateau, as highlighted in Fig. 2a and Supplementary Fig.

https://doi.org/10.5194/egusphere-2026-3511
Preprint. Discussion started: 29 June 2026

S4. This spatial correspondence emphasizes the role of rough topography and boundary-intensified mixing in concentrating abyssal upwelling into localized hotspots, rather than distributing it evenly across basin interiors (Baker et al., 2023; Ferrari, 2014; Ferrari et al., 2016; Ledwell et al., 2000; Wynne-Cattanach et al., 2024).

Having established the horizontal localization of abyssal diapycnal exchange, we next examine its large-scale vertical and basin-scale organization using the 30-year mean zonal-mean diapycnal velocity fields shown in Fig. 2b-e. These fields identify where the circulation supports upward or downward transfer across density classes. The most coherent cross-isopycnal structures are organized around the upper-ocean wind-driven circulation, the Southern Ocean overturning regime, and selected high-latitude formation regions. In the upper ocean, the pattern resembles the familiar wind-driven structure, with equatorial upwelling flanked by subtropical downwelling. Deeper in the water column, the signal becomes more selective and highlights where the lower overturning cell communicates most readily with lighter density classes.

Between about 40° S and 40° N in the upper ocean (γ^n < 26 kg m^{-3}; Supplementary Fig. S3), the zonal-mean pattern is consistent with the large-scale vertical-velocity structure associated with wind-driven circulation, with equatorial upwelling and subtropical downwelling (Liang et al., 2017). The same diagnostic also exposes the deeper density classes relevant to abyssal return. Particularly noteworthy is the near-continuous equatorial upwelling signal from the deep ocean toward the surface in the Pacific and Indian basins, whereas the equatorial Atlantic shows much weaker vertical coherence.

At northern high latitudes, the Atlantic exhibits pronounced downwelling extending to about $\gamma^n \approx 28.0$ kg m^{-3} (roughly 2000 m; Supplementary Fig. S3), consistent with North Atlantic Deep Water (NADW) formation. By contrast, the North Pacific shows weaker mid- and deep-layer diapycnal motion, consistent with stronger stratification and the confinement of vigorous downwelling to the upper ocean, where North Pacific Intermediate Water forms. These basin differences already suggest that the upward return of bottom waters will not be organized identically across the global ocean.

The clearest large-scale signature relevant to abyssal return occurs in the Southern Hemisphere. A vertically coherent dipole structure is evident across the Antarctic Circumpolar Current (ACC), characterized by downwelling near the Antarctic margin and upwelling farther north within the ACC belt (Fig. 2b-e). This dipole provides a physical bridge between local transformation and large-scale return: wind-driven divergence and isopycnal outcropping in the ACC belt can expose transformed abyssal waters to lighter density classes, whereas near-Antarctic downwelling and dense-water formation continually resupply the abyssal reservoir. The density-space dipole is consistent with the Southern Ocean's central role in lower-cell closure and with the spiraling ascent pathways identified in earlier tracer analyses (Ferrari, 2014; Marshall and Speer, 2012; Talley, 2013; Tamsitt et al., 2017).

Together, the spatial and zonal-mean diapycnal velocity fields in Fig. 2 define the dynamical framework for the pathway diagnostics examined in Sect. 3.2. Southern Ocean upwelling provides the dominant large-scale return gateway, while equatorial and boundary-associated regions contribute additional localized routes for cross-isopycnal ascent.

https://doi.org/10.5194/egusphere-2026-3511
Preprint. Discussion started: 29 June 2026

3.2 Pathways of Global Ocean Bottom Water Ventilation

Having established where cross-isopycnal exchange is dynamically favored, we next examine how bottom-water signals accumulate, spread, and are transformed away from the abyss. Section 3.2 combines three complementary diagnostics: ventilation thickness, which measures the column-integrated imprint of bottom-water influence; concentration distribution, which resolves the density-space geometry of the return pathways; and concentration-weighted diapycnal flux, which links that geometry to transport intensity. Interpreted together, these fields show not only where bottom-water influence is present, but also how far it penetrates into lighter density classes and where upward transformation is most effective.

Ventilation thickness is defined as the vertical integral of seawater concentration over the local water column, $T = \int_{z\_b}^{z\_s} C\, dz$, where z_b and z_s denote the local bottom and surface levels, respectively. Here, C is the dimensionless seawater concentration introduced above and represents the fraction of bottom water at each location. Although T therefore has units of meters, it does not represent an actual physical depth; rather, it quantifies the vertically integrated influence of bottom-water signals throughout the water column at each horizontal location. Considered together with the quasi-equilibrium concentration fields and the concentration-weighted diapycnal fluxes, ventilation thickness provides a compact view of where abyssal return first emerges, how broadly it expands, and where it is expressed most strongly through the full water column.

The evolution of ventilation thickness after 1, 10, 50, and 100 years of integration is shown in Fig. 3. The sequence reveals a clear spatio-temporal progression: early bottom-water influence remains confined to a limited set of regions, whereas on multidecadal timescales it expands into a broader but still highly heterogeneous global footprint.

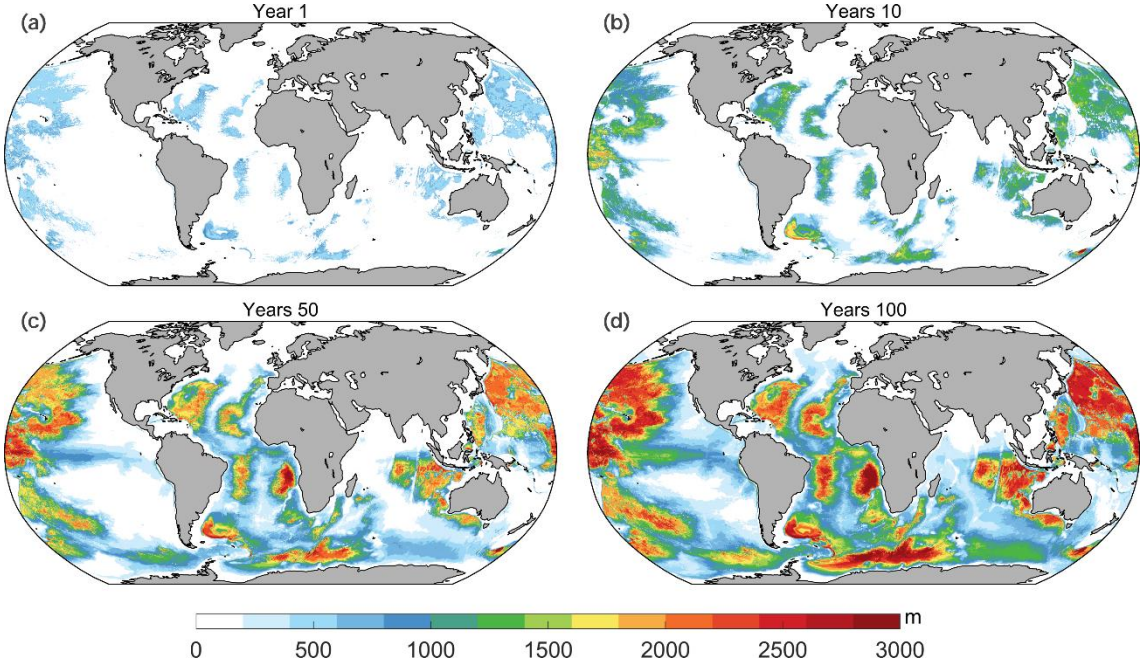

https://doi.org/10.5194/egusphere-2026-3511
Preprint. Discussion started: 29 June 2026

Figure 3 Global distribution of bottom-water ventilation thickness (m) after (a) 1 year, (b) 10 years, (c) 50 years, and (d) 100 years of integration. Ventilation thickness is the vertical integral of bottom-water concentration and represents the column-integrated influence of bottom-water signals.

During the initial stages (years 1 and 10; Fig. 3a, b), substantial ventilation thickness is concentrated mainly in the Southern Ocean and in a limited number of boundary-associated regions. These early signals coincide closely with the areas of intense diapycnal exchange identified in Fig. 2, especially the Southern Ocean topographic hotspots and selected deep boundary pathways. This correspondence indicates that the initial spread of bottom-water influence is preferentially organized by localized regions where cross-isopycnal transformation is strongest (Baker et al., 2023; Ferrari, 2014; Ferrari et al., 2016; Ledwell et al., 2000; Wynne-Cattanach et al., 2024).

By 50 and 100 years (Fig. 3c, d), the ventilated footprint expands across all major basins, but the distribution remains strongly uneven. The Southern Ocean continues to exhibit the largest and most coherent ventilation thickness, including pronounced signals near Drake Passage and the Weddell Sea, while secondary maxima emerge in the tropical-subtropical Pacific, along parts of the Atlantic western boundary system, and in the southern Indian Ocean. These patterns indicate that abyssal return is globally connected but highly uneven in its spatial expression, with bottom-water influence accumulating preferentially in a limited number of dynamically active regions, whereas other areas remain only weakly affected even after a century of integration.

Viewed on its own, ventilation thickness identifies the vertically integrated footprint of abyssal return, but it does not distinguish how that return is organized in density space or how it differs among basins. The zonal-mean concentration fields in Fig. 4 provide that next step by resolving the large-scale pathway geometry of bottom-water ascent and clarifying where bottom-water influence most effectively enters lighter density classes.

Diagnosed at quasi-equilibrium using the criteria described in Sect. 2.1, the zonal-mean concentration field provides a basin-comparative view of bottom-water return pathways (Fig. 4). Whereas ventilation thickness emphasizes the vertically integrated strength of bottom-water influence, the concentration field resolves the density-space geometry of the return pathways and therefore reveals how bottom-water signals rise and spread through the Atlantic, Pacific, and Indian Oceans.

The global field shows that the Southern Ocean is the dominant return hub in this analysis (Fig. 4a). Bottom-water signals rise from the densest classes and spread upward and equatorward, with the 0.2-0.4 contours extending toward the upper branch of the deep overturning. This pattern is consistent with the view that Antarctic Bottom Water formed around Antarctica is transformed upward through a combination of Southern Ocean upwelling and isopycnal export (Ferrari, 2014; Orsi et al., 1999; Talley, 2013; Tamsitt et al., 2017). The broad outcropping of the 0.2 contour across Southern Ocean sectors further indicates that bottom-water return to the upper ocean is not confined to a single longitude band, but occurs around much of the circumpolar domain.

https://doi.org/10.5194/egusphere-2026-3511
Preprint. Discussion started: 29 June 2026

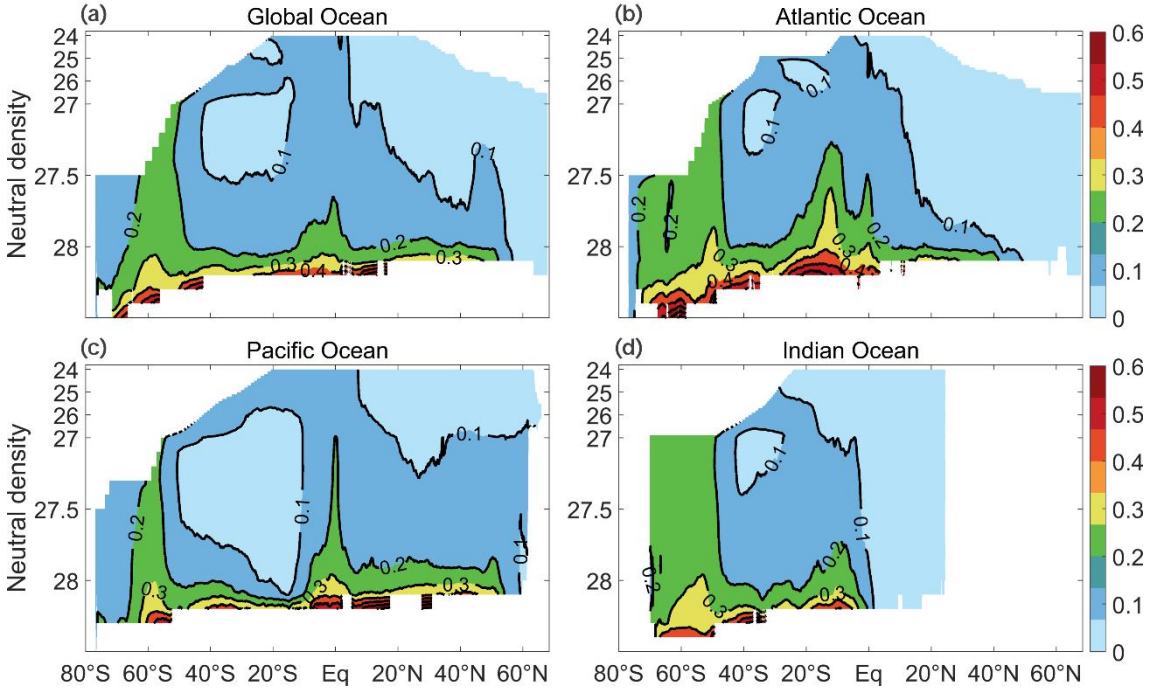

Figure 4 Zonal-mean distributions of bottom-water concentration in the (a) global ocean, (b) Atlantic Ocean, (c) Pacific Ocean, and (d) Indian Ocean. Concentration is a dimensionless quantity representing the fraction of water originating from the model bottom layer. Shading indicates the concentration field, while black contours denote concentration isolines and highlight the vertical extent and pathway structure of bottom-water influence across the major ocean basins.

Marked inter-basin contrasts emerge once the analysis is separated by basin. In the Atlantic (Fig. 4b), bottom-water signals are strongest and occupy the broadest vertical range, with high concentration values extending farthest toward lighter density classes. The wide outcropping of the 0.2 contour in the Southern Hemisphere and the substantial penetration of concentration signals into the subtropical and mid-latitude Atlantic indicate an efficient return pathway superimposed on the basin's vigorous overturning structure. Compared with the Pacific and Indian Oceans, the Atlantic therefore shows the clearest combination of strong bottom-water influence and substantial upward reach. This interpretation is consistent with the strong ventilation-thickness signals in the South Atlantic and Weddell-connected sectors (Fig. 3d).

The Pacific exhibits a contrasting structure. Although bottom-water signals clearly enter the basin from the south, most of the concentration remains confined to deep density classes (Fig. 4c), indicating weaker upward penetration into lighter waters than in the Atlantic. The main exception occurs in the equatorial Pacific, where the 0.2 contour rises markedly upward, consistent with the coherent equatorial upwelling structure in Fig. 2d. Broad deep retention and localized equatorial ascent together indicate that the Pacific acts as a major reservoir of old bottom waters, with only selected pathways providing efficient escape toward the upper ocean (Shah et al., 2017; Talley, 2013; Tamsitt et al., 2017).

The Indian Ocean lies between these two end members. Its concentration field (Fig. 4d) does not show the broad, strong upward penetration seen in the Atlantic, but neither is it as uniformly confined to deep layers as in much of the Pacific. In

https://doi.org/10.5194/egusphere-2026-3511
Preprint. Discussion started: 29 June 2026

addition to the Southern Ocean sector, a clear upward signal of bottom-water influence is also evident in the southern subtropical Indian Ocean, where a localized concentration maximum aligns with the region of enhanced ventilation thickness identified in Fig. 3d. These patterns indicate that bottom-water return in the Indian basin is expressed through a more spatially focused pathway structure, likely linked to the combined influence of Southern Ocean connection and regional ridge-associated transformation rather than basin-wide ascent.

Overall, the concentration fields reveal a globally connected but strongly asymmetric return structure. The Southern Ocean provides the dominant large-scale gateway by which bottom-water influence re-enters lighter density classes, but the efficiency and vertical reach of that return differ sharply among basins. This inter-basin contrast becomes clearest when the density-space diagnostics are viewed together with the map-based measures of ventilation thickness and flux.

To connect the pathway patterns identified above with cross-isopycnal transport, we diagnose a concentration-weighted analogue of the water-mass transformation rate (WMT), which is commonly defined as the integral of diapycnal velocity across isopycnal surfaces (Cimoli et al., 2023; Ferrari et al., 2016). In the present context, this weighting isolates where transformation acts most effectively on bottom-water influence rather than on the full water-mass field. The concentration-weighted diapycnal flux is defined as

$$\Phi_C = \iint_{A(\rho)} \omega_d \cdot n_\rho \cdot C \, dxdy \tag{5}$$

where $A(\rho)$ denotes the area of a given isopycnal surface, ω_d is the diagnosed diapycnal velocity, n_ρ is the unit normal vector to the density surface, and C is the bottom-water concentration.

Physically, Φ_C measures the component of diapycnal transport that carries a bottom-water signal. It therefore differs from a conventional water-mass transformation diagnostic by weighting the diapycnal exchange with the fraction of bottom-water origin. Regions with strong diapycnal velocity but weak bottom-water concentration contribute little to Φ_C, whereas regions where upward diapycnal motion coincides with high bottom-water concentration make the largest contribution to the transformation of bottom-water influence. Here positive values indicate transport toward denser classes (downwelling), whereas negative values indicate transport toward lighter classes (upwelling). Interpreted together with the concentration fields, this diagnostic identifies where upward transformation of bottom-water influence is strongest and thereby helps explain the pathway geometry seen in Fig. 4.

Strong upwelling diapycnal concentration fluxes in Fig. 5a are concentrated in the Southern Ocean, the equatorial Pacific, and parts of the equatorial Atlantic. These flux maxima coincide with regions that either exhibit vigorous localized diapycnal exchange (Fig. 2) or stand out in the concentration and ventilation-thickness fields (Figs. 3 and 4). In the Southern Ocean, the strongest upward fluxes align with Drake Passage, the Kerguelen Plateau, and the Campbell Plateau sectors, reinforcing the inference that rough topography and associated mixing hotspots organize a substantial fraction of abyssal return (Baker et al., 2023; Ferrari, 2014; Ferrari et al., 2016; Ledwell et al., 2000; Wynne-Cattanach et al., 2024).

The density-integrated view (Fig. 5b) further clarifies where this transformation is concentrated. Upwelling fluxes dominate in the abyssal density range above about γ^n = 28.0 kg m^{-3}, whereas the net flux approaches zero in the overlying deep ocean,

https://doi.org/10.5194/egusphere-2026-3511
Preprint. Discussion started: 29 June 2026

consistent with a transition from active cross-isopycnal lifting of bottom-water influence to subsequent along-isopycnal spreading. Dense bottom waters are thus first lifted upward by diapycnal mixing and then continue their return pathway along lighter density surfaces (Ferrari, 2014; Ferrari et al., 2016; Talley, 2013).

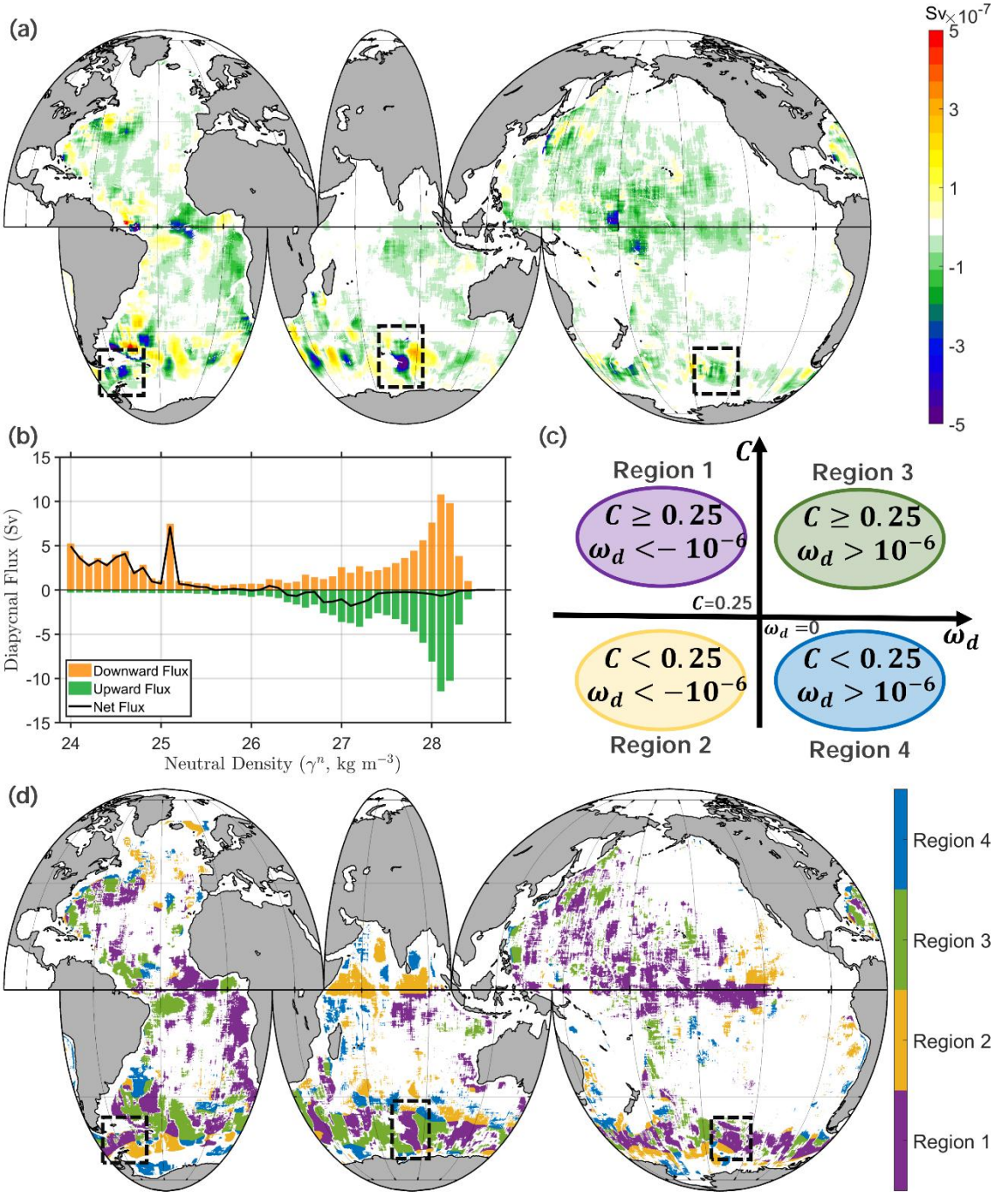

https://doi.org/10.5194/egusphere-2026-3511
Preprint. Discussion started: 29 June 2026

Figure 5 Concentration-weighted diapycnal flux and the coupling between diapycnal motion and bottom-water concentration. (a) Global distribution of concentration-weighted diapycnal flux (Sv) on the neutral-density surface $\gamma^n = 28.1\ \mathrm{kg\,m^{-3}}$. Positive values indicate transport toward denser classes (downwelling), whereas negative values indicate transport toward lighter classes (upwelling). Black dashed boxes mark representative Southern Ocean hotspots of intensified upward transformation. (b) Integrated concentration-weighted diapycnal fluxes across different neutral-density surfaces, including upwelling fluxes (green), downwelling fluxes (yellow), and net fluxes (black). (c) Schematic classification of four dynamical–tracer regimes based on bottom-water concentration (C) and diapycnal velocity (ω_d). The thresholds ($C = 0.25$) and ($|\omega_d| = 10^{-6}\ \mathrm{m\,s^{-1}}$) separate regions of strong or weak bottom-water influence and upward or downward diapycnal motion. (d) Global distribution of the four regimes on the $\gamma^n = 28.1\ \mathrm{kg\,m^{-3}}$ surface. White areas indicate regions outside the classified effective range.

We also examine the available area of each neutral-density surface, because the magnitude of the integrated transformation depends not only on the local strength of cross-isopycnal exchange but also on the area over which that exchange occurs. The available surface area increases sharply from the abyss toward $\gamma^n \approx 28.0\ \mathrm{kg\ m^{-3}}$, after which it varies much more gradually (Supplementary Fig. S5). The strongest transformation of bottom-water influence therefore occurs where substantial cross-isopycnal exchange coincides with rapidly increasing surface area. The concentration-weighted flux diagnostics support the same central interpretation as Figs. 3 and 4: abyssal return is concentrated in a limited set of dynamically favored regions and density classes rather than being distributed uniformly through the global ocean.

Motivated by Eq. (5), we further examine the local coupling between diapycnal motion and bottom-water concentration on the $\gamma^n = 28.1\ \mathrm{kg\,m^{-3}}$ surface. This analysis separates regions where diapycnal exchange is dynamically active from regions where that exchange acts directly on water that still carries a substantial bottom-water signal. We classify the valid grid points into four regimes using $C = 0.25$ as the concentration threshold and $|\omega_d| = 10^{-6}\ \mathrm{m\,s^{-1}}$ as the velocity threshold (Fig. 5c). Region 1 ($C \geq 0.25$, $\omega_d < -10^{-6}\ \mathrm{m\,s^{-1}}$) represents the most effective upward bottom-water transformation regime, where strong bottom-water influence coincides with diapycnal motion toward lighter density classes. Region 2 ($C < 0.25$, $\omega_d < -10^{-6}\ \mathrm{m\,s^{-1}}$) identifies upward diapycnal motion that carries only a weak bottom-water signal. Region 3 ($C \geq 0.25$, $\omega_d > 10^{-6}\ \mathrm{m\,s^{-1}}$) marks regions where bottom-water-influenced waters are associated with downward transformation or local recirculation toward denser classes. Region 4 ($C < 0.25$, $\omega_d > 10^{-6}\ \mathrm{m\,s^{-1}}$) corresponds to downwelling regions with weak bottom-water influence.

The spatial distribution of these regimes (Fig. 5d) shows that Region 1 is not confined to isolated diapycnal velocity hotspots, but occupies broad portions of the effective area on the $\gamma^n = 28.1\ \mathrm{kg\,m^{-3}}$ surface, accounting for 44.8% of that area. Region 1 is especially prominent in the Southern Ocean and in pathways extending into the major basins, consistent with the concentration structure in Fig. 4 and the enhanced upward diapycnal exchange identified in Fig. 2. This indicates that the most dynamically relevant bottom-water return occurs where upward diapycnal motion overlaps with appreciable bottom-water concentration. By contrast, Region 2 highlights areas where upwelling is dynamically present but contributes less directly to bottom-water return because the bottom-water signal is weak, such as in parts of the northern Indian Ocean.

Regions 3 and 4 show that downwelling motions can occur both within and outside bottom-water-influenced pathways, emphasizing that diapycnal velocity alone is insufficient to diagnose abyssal return. In the Southern Ocean, Regions 1 and 3 occur close to each other, indicating that bottom-water-influenced waters can experience both upward and downward

https://doi.org/10.5194/egusphere-2026-3511
Preprint. Discussion started: 29 June 2026

cross-isopycnal motions within the same broad return pathway. This patchy arrangement suggests that the upward return of abyssal waters is not strictly monotonic, but may involve alternating transformation and spreading along complex pathways, consistent with the spiraling ascent toward the Southern Ocean surface described by Tamsitt et al. (2017). The quadrant analysis therefore supports the role of Φ_C as a bridge between the dynamical field and the tracer field: effective bottom-water transformation requires both diapycnal motion and a substantial bottom-water-origin signal.

Ventilation thickness, concentration distribution, and concentration-weighted diapycnal flux together define a physically coherent pathway structure for abyssal return. The Southern Ocean provides the dominant large-scale gateway, while equatorial and boundary-associated routes contribute more localized branches. Viewed collectively, these diagnostics relate pathway geometry, column-integrated influence, and cross-isopycnal transformation within one global description.

3.3 Time Scales of Global Ocean Bottom Water Ventilation

Section 3.2 resolved the geometry of bottom-water return pathways; we now examine how rapidly those pathways operate. Water age is a standard tracer-based measure of ventilation timescale (England, 1995; Fine et al., 2017; Waugh et al., 2003), and, when interpreted together with concentration, distinguishes regions where bottom-water influence is present from regions where that influence is renewed efficiently. The age field thus provides the temporal counterpart to the pathway structure diagnosed above and allows the basin asymmetry of abyssal return to be evaluated within one consistent framework.

Based on the operational criteria introduced in Sect. 2.1, we estimated a quasi-equilibrated water-age field over a centennial timescale. The zonal-mean distributions for the global ocean and the three major basins are shown in Fig. 6. At the global scale (Fig. 6a), the youngest ages are concentrated in the Southern Ocean and adjacent ACC sectors, where bottom-water influence also rises most effectively toward the surface in Fig. 4a. This correspondence between strong concentration and young age identifies the Southern Ocean as the dominant return hub, consistent with the leading role of Southern Ocean upwelling in lower-cell closure (Ferrari, 2014; Marshall and Speer, 2012; Talley, 2013; Tamsitt et al., 2017). Age increases away from these sectors along the upward-spreading density pathways, indicating that the principal Southern Ocean branches of abyssal return operate on timescales of several decades and extend to roughly 70-80 years along the longer zonal-mean pathways resolved here, broadly consistent with previous trajectory-based estimates (Tamsitt et al., 2017).

In the Atlantic (Fig. 6b), ages remain relatively young south of about 40° S but increase to about 40-60 years at mid-latitudes and exceed about 80 years toward the northern high latitudes. This meridional aging pattern mirrors the concentration structure in Fig. 4b: bottom-water influence penetrates upward efficiently through the Southern Ocean and South Atlantic, while farther northward renewal is increasingly shaped by the strong downwelling branch associated with NADW formation (Fig. 2c) (Lumpkin and Speer, 2007; Talley, 2013). The Atlantic therefore combines the strongest vertical imprint of bottom-water return with a pronounced northward aging gradient, indicating that pathway strength and renewal rate vary substantially within the basin.

https://doi.org/10.5194/egusphere-2026-3511
Preprint. Discussion started: 29 June 2026

The Pacific exhibits the clearest contrast between pathway presence and temporal efficiency. Bottom-water influence clearly enters the basin from the south and remains visible in Fig. 4c, yet age increases rapidly northward and exceeds about 80 years over much of the basin, locally approaching 100 years in the northern interior (Fig. 6c). This old-age structure is consistent with the basin's strong stratification and comparatively weak deep overturning, which limit upward renewal once bottom waters leave the Southern Ocean source sectors (Talley, 2013; Tamsitt et al., 2017). The main exception is the equatorial Pacific, where comparatively young ages coincide with the coherent upwelling signatures in Figs. 2d, 3, and 5. The equatorial Pacific therefore appears less as a broad return hub than as a localized leakage route that partially relieves otherwise slow basin-scale renewal, consistent with previous analyses of North Pacific deep-water ventilation pathways (Shah et al., 2017).

The Indian Ocean occupies an intermediate position between the Atlantic and Pacific end members. Ages are generally older than in the Atlantic but younger and more spatially structured than in the Pacific (Fig. 6d). Despite coherent diapycnal motion near the equator, the strongest younger-age corridor occurs in the subtropical southern Indian Ocean, where reduced ages align with the concentration enhancement in Fig. 4d and with the pronounced ventilation-thickness hotspot near the ridge system in Fig. 3d. This coherence across diagnostics suggests that ridge-associated and subtropical pathways provide the most effective Indian Ocean branches of abyssal return in the diagnosed fields. By contrast, the northern Indian Ocean retains ages mostly above about 80 years, indicating weak renewal of bottom-water influence there.

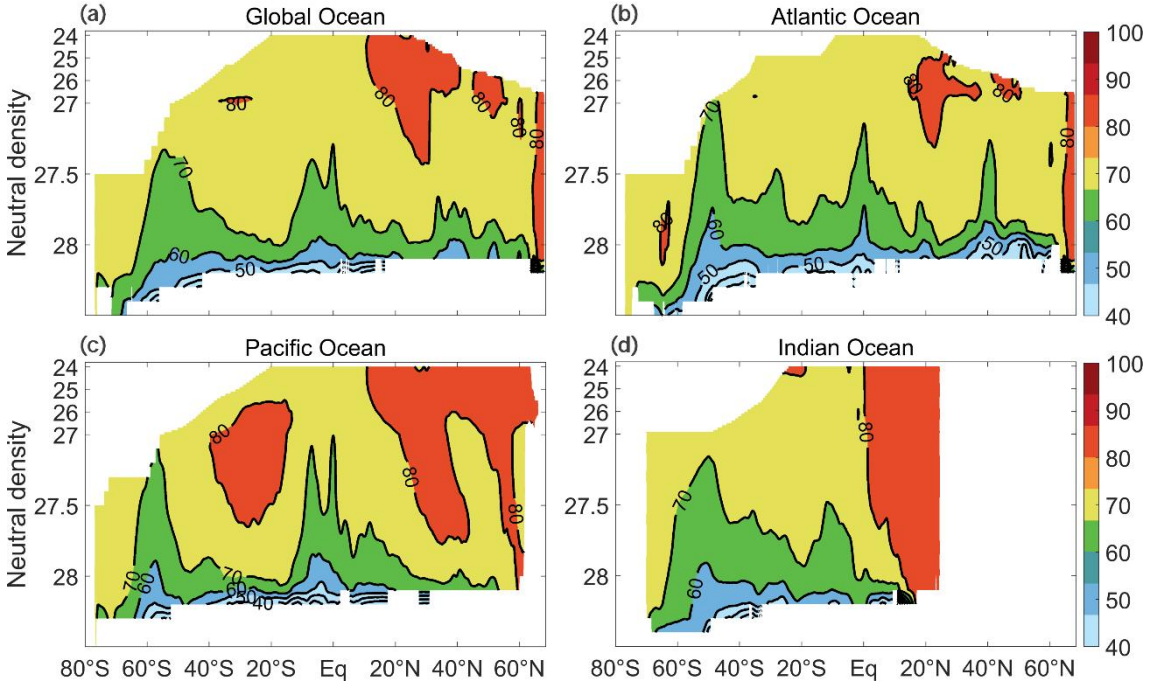

Figure 6 Zonal-mean distributions of bottom-water ventilation age (years) in the (a) global ocean, (b) Atlantic Ocean, (c) Pacific Ocean, and (d) Indian Ocean. Shading indicates the age field and highlights the contrasting renewal timescales of abyssal return among the major ocean basins.

https://doi.org/10.5194/egusphere-2026-3511
Preprint. Discussion started: 29 June 2026

The age diagnostics provide the temporal counterpart to the pathway structure identified in Sect. 3.2. The same basin hierarchy appears in both views: the Southern Ocean dominates the large-scale return of bottom-water influence, the Atlantic supports the strongest upward penetration but with substantial northward aging, the Pacific acts as the principal reservoir of old bottom waters, and the Indian Ocean contains more localized return corridors. The agreement among concentration, ventilation thickness, flux, and age diagnostics shows that the global asymmetry of abyssal return is expressed not only in pathway geometry but also in renewal timescale.

4 Discussion

The results resolve a strongly asymmetric global return structure rather than a spatially uniform or single diffuse upwelling branch. The Southern Ocean acts as the dominant large-scale return hub, while the Atlantic, Pacific, and Indian basins express different combinations of upward reach, column-integrated imprint, transformation intensity, and renewal timescale. This synthesis is consistent with the long-standing view that Southern Ocean upwelling is central to the closure of the lower overturning circulation (Ferrari, 2014; Marshall and Speer, 2012; Talley, 2013), and extends that view by showing how topographic, equatorial, and boundary-associated pathways shape the basin-scale expression of bottom-water return.

This basin asymmetry places the diagnosed return structure in the context of earlier work. Previous studies established key elements of the abyssal return problem, including enhanced cross-isopycnal exchange over rough topography and boundaries (Holmes et al., 2019; Ledwell et al., 2000; McDougall and Ferrari, 2017; Ruan and Ferrari, 2021; Wynne-Cattanach et al., 2024), spiraling ascent pathways into the Southern Ocean surface (Tamsitt et al., 2017), and equatorial leakage routes for North Pacific deep waters (Shah et al., 2017). The present analysis integrates these process-based insights within a common global comparison. The diagnostics presented in Figs. 2-5 show that dynamically active regions also organize the strongest bottom-water concentration signals and concentration-weighted transformation. These pathway differences are further reflected in basin-scale contrasts in renewal timescale, as revealed by the concentration and water-age distributions (Figs. 4 and 6). Interpreting pathway geometry, column imprint, cross-isopycnal transformation, and age together yields a consistent global comparison of abyssal return.

The four diagnostics resolve different dimensions of abyssal return. Ventilation thickness (Fig. 3) identifies where bottom-water influence accumulates through the full water column. Concentration (Fig. 4) resolves the large-scale geometry of upward penetration into lighter classes, whereas concentration-weighted diapycnal flux (Fig. 5) links that geometry to the locations and density ranges where cross-isopycnal transformation is most effective. Water age (Fig. 6) provides the temporal counterpart by distinguishing rapidly renewed pathways from slowly ventilated reservoirs (England, 1995; Fine et al., 2017; Waugh et al., 2003). The convergence of these four diagnostics on the same basin hierarchy--Southern Ocean dominance, strong Atlantic upward reach, persistent Pacific aging, and more localized Indian renewal corridors--strengthens the physical interpretation.

https://doi.org/10.5194/egusphere-2026-3511
Preprint. Discussion started: 29 June 2026

The analysis is based on the GLORYS12 reanalysis (Artana et al., 2021; Jean-Michel et al., 2021; Lellouche et al., 2018; Verezemskaya et al., 2021) and climatological forcing within the CART framework, so the diagnosed fields describe the large-scale return structure resolved by this framework. The concentration thresholds and quasi-equilibrium criteria introduced in Sect. 2.1 focus the analysis on the dominant pathway and renewal-time structure, while the concentration-weighted flux in Fig. 5 complements standard water-mass transformation perspectives by isolating the component of diapycnal exchange that carries bottom-water influence (Cimoli et al., 2023; Ferrari et al., 2016). Regional interpretations involving boundary currents, ridge systems, or overlying deep-water formation are therefore drawn from the combined evidence of the diagnostics and the existing literature. The close agreement among Figs. 2-6 indicates that the first-order asymmetry of abyssal return is a coherent feature of the diagnosed circulation.

These results have broader implications for how the lower overturning circulation reconnects abyssal waters to the upper ocean. Because bottom-water return is concentrated in a limited set of Southern Ocean, equatorial, and topographically influenced pathways, the climatic and biogeochemical impacts of abyssal renewal depend not only on the total overturning strength but also on how these geographically distinct pathways respond to changing winds, stratification, and mixing (Cessi, 2019; Lee et al., 2023; Lumpkin and Speer, 2007; Morrison et al., 2022; Purkey et al., 2018). Future time-dependent pathway analyses, targeted sensitivity experiments, and observational constraints can test how stable these basin contrasts remain under interannual-to-decadal variability and future climate change.

5 Conclusions

In this study, we combined a high-resolution global ocean reanalysis with CART to diagnose bottom-water return from complementary perspectives of vertically integrated influence, pathway geometry, cross-isopycnal transformation, and ventilation timescale. Joint analysis of ventilation thickness, concentration distribution, concentration-weighted diapycnal flux, and water age provides a physically connected global diagnosis of where bottom-water signals spread, where they are transformed most effectively across density surfaces, and how rapidly they return toward the upper ocean.

Our results show that global bottom-water return is strongly asymmetric rather than basin-uniform. The Southern Ocean emerges as the dominant return hub, with broad outcropping pathways and young ages that together indicate the most efficient linkage between abyssal waters and the upper ocean (Figs. 4 and 6). At the same time, the Atlantic, Pacific, and Indian Oceans exhibit distinct pathway geometries and timescales: the Atlantic shows comparatively strong and broad return signatures, the Pacific retains older bottom-water influence under stronger stratification, and the Indian Ocean contains more localized subtropical and ridge-associated return corridors. Read together with the integrated diagnostics of ventilation thickness and concentration-weighted diapycnal flux (Figs. 3 and 5), these patterns indicate that abyssal return is organized by the combined effects of Southern Ocean upwelling, rough-topography mixing, equatorial upwelling, and basin-specific overturning structure.

https://doi.org/10.5194/egusphere-2026-3511
Preprint. Discussion started: 29 June 2026

By combining pathway geometry, cross-isopycnal transformation, and return timescale within a single global diagnostic framework, this study sharpens the view of lower-cell closure and of how abyssal waters reconnect with the upper ocean. The results show that bottom-water return is globally connected yet strongly basin-asymmetric in both efficiency and timing. Future work can further test the sensitivity of these results to threshold choices, forcing strategy, and unresolved mixing processes, while integrating long-term observations to better constrain the role of bottom-water ventilation in climate and biogeochemical redistribution.

Code and data availability

The GLORYS12 ocean reanalysis product data are available from https://resources.marine.copernicus.eu/product/GLOBAL_MULTIYEAR_PHY_001_030/. The processed data and analysis scripts used here and supplementary materials are available at https://doi.org/10.5281/zenodo.20688093.

Supplement link

The supplementary material is published as separate file alongside this article.

Author contributions

GC and ZQ conceived the study and designed its overall objectives. ZQ designed the experiments. GC conducted the data analysis and produced the first draft of the manuscript. ZQ and ZY interpreted the results and edited the manuscript. All authors proof read the manuscript before submission.

Competing interests

The contact author has declared that none of the authors has any competing interests.

Acknowledgements

This work was supported by CORE, a joint research center for ocean research between Laoshan Laboratory and the Hong Kong University of Science and Technology, with substantial support from the Research Grants Council of the Hong Kong Special Administrative Region, China (Project Reference No. AoE/P-601/23-N).

https://doi.org/10.5194/egusphere-2026-3511
Preprint. Discussion started: 29 June 2026

Financial support

This work was supported by the National Natural Science Foundation of China (Nos. 42450181, 42276004, and 42376024), the Science and Technology Development Fund, Macau (001/2024/SKL), and the Centre for Regional Oceans, University of Macau (SP2025-00005-CRO).

References

Artana, C., Ferrari, R., Bricaud, C., Lellouche, J.-M., Garric, G., Sennéchael, N., Lee, J.-H., Park, Y.-H., and Provost, C.: Twenty-five years of Mercator ocean reanalysis GLORYS12 at Drake Passage: Velocity assessment and total volume transport, Advances in Space Research, 68, 447–466, https://doi.org/10.1016/j.asr.2019.11.033, 2021.

Baker, L. E., Mashayek, A., and Naveira Garabato, A. C.: Boundary Upwelling of Antarctic Bottom Water by Topographic Turbulence, AGU Advances, 4, e2022AV000858, https://doi.org/10.1029/2022AV000858, 2023.

Bennett, S. L.: The Relationship between Vertical, Diapycnal, and Isopycnal Velocity and Mixing in the Ocean General Circulation, J. Phys. Oceanogr., 16, 167–174, https://doi.org/10.1175/1520-0485(1986)016<0167:TRBVDA>2.0.CO;2, 1986.

Blanke, B., Speich, S., Madec, G., and Maugé, R.: A global diagnostic of interior ocean ventilation, Geophysical Research Letters, 29, 1267, https://doi.org/10.1029/2001GL013727, 2002.

Cessi, P.: The Global Overturning Circulation, Annu. Rev. Mar. Sci., 11, 249–270, https://doi.org/10.1146/annurev-marine-010318-095241, 2019.

Cimoli, L., Mashayek, A., Johnson, H. L., Marshall, D. P., Naveira Garabato, A. C., Whalen, C. B., Vic, C., De Lavergne, C., Alford, M. H., MacKinnon, J. A., and Talley, L. D.: Significance of Diapycnal Mixing Within the Atlantic Meridional Overturning Circulation, AGU Advances, 4, e2022AV000800, https://doi.org/10.1029/2022AV000800, 2023.

De Lavergne, C., Madec, G., Le Sommer, J., Nurser, A. J. G., and Naveira Garabato, A. C.: On the Consumption of Antarctic Bottom Water in the Abyssal Ocean, Journal of Physical Oceanography, 46, 635–661, https://doi.org/10.1175/JPO-D-14-0201.1, 2016.

De Lavergne, C., Madec, G., Roquet, F., Holmes, R. M., and McDougall, T. J.: Abyssal ocean overturning shaped by seafloor distribution, Nature, 551, 181–186, https://doi.org/10.1038/nature24472, 2017.

Deleersnijder, E., Campin, J.-M., and Delhez, E. J. M.: The concept of age in marine modelling I. Theory and preliminary model results, J. Mar. Syst., 28, 229–267, https://doi.org/10.1016/S0924-7963(01)00026-4, 2001.

Delhez, E. J. M.: Transient residence and exposure times, Ocean Science, 2, 1–9, https://doi.org/10.5194/os-2-1-2006, 2006.

Delhez, E. J. M., Campin, J.-M., Hirst, A. C., and Deleersnijder, E.: Toward a general theory of the age in ocean modelling, Ocean Modelling, 1, 17–27, https://doi.org/10.1016/S1463-5003(99)00003-7, 1999.

Du Pontavice, H., Chen, Z., and Saba, V. S.: A high-resolution ocean bottom temperature product for the northeast U.S. continental shelf marine ecosystem, Progress in Oceanography, 210, 102948, https://doi.org/10.1016/j.pocean.2022.102948, 2023.

https://doi.org/10.5194/egusphere-2026-3511
Preprint. Discussion started: 29 June 2026

England, M. H.: The Age of Water and Ventilation Timescales in a Global Ocean Model, Journal of Physical Oceanography, 25, 2756–2777, https://doi.org/10.1175/1520-0485(1995)025%253C2756:TAOWAV%253E2.0.CO;2, 1995.

Ferrari, R.: What goes down must come up, Nature, 513, 179–180, https://doi.org/10.1038/513179a, 2014.

Ferrari, R., Mashayek, A., McDougall, T. J., Nikurashin, M., and Campin, J.-M.: Turning Ocean Mixing Upside Down, Journal of Physical Oceanography, 46, 2239–2261, https://doi.org/10.1175/JPO-D-15-0244.1, 2016.

Ferrari, R., Nadeau, L.-P., Marshall, D. P., Allison, L. C., and Johnson, H. L.: A Model of the Ocean Overturning Circulation with Two Closed Basins and a Reentrant Channel, Journal of Physical Oceanography, 47, 2887–2906, https://doi.org/10.1175/JPO-D-16-0223.1, 2017.

Fine, R. A., Peacock, S., Maltrud, M. E., and Bryan, F. O.: A new look at ocean ventilation time scales and their uncertainties, JGR Oceans, 122, 3771–3798, https://doi.org/10.1002/2016JC012529, 2017.

Gunn, K. L., Rintoul, S. R., England, M. H., and Bowen, M. M.: Recent reduced abyssal overturning and ventilation in the Australian Antarctic Basin, Nat. Clim. Chang., 13, 537–544, https://doi.org/10.1038/s41558-023-01667-8, 2023.

Holmes, R. M., De Lavergne, C., and McDougall, T. J.: Tracer Transport within Abyssal Mixing Layers, Journal of Physical Oceanography, 49, 2669–2695, https://doi.org/10.1175/JPO-D-19-0006.1, 2019.

Jackett, D. R. and McDougall, T. J.: A Neutral Density Variable for the World's Oceans, Journal of Physical Oceanography, 27, 237–263, https://doi.org/10.1175/1520-0485(1997)027<0237:ANDVFT>2.0.CO;2, 1997.

Jean-Michel, L., Eric, G., Romain, B.-B., Gilles, G., Angélique, M., Marie, D., Clément, B., Mathieu, H., Olivier, L. G., Charly, R., Tony, C., Charles-Emmanuel, T., Florent, G., Giovanni, R., Mounir, B., Yann, D., and Pierre-Yves, L. T.: The Copernicus Global 1/12° Oceanic and Sea Ice GLORYS12 Reanalysis, Front. Earth Sci., 9, 698876, https://doi.org/10.3389/feart.2021.698876, 2021.

Large, W. G., McWilliams, J. C., and Doney, S. C.: Oceanic vertical mixing: A review and a model with a nonlocal boundary layer parameterization, Reviews of Geophysics, 32, 363–403, https://doi.org/10.1029/94RG01872, 1994.

Ledwell, J. R., Montgomery, E. T., Polzin, K. L., St. Laurent, L. C., Schmitt, R. W., and Toole, J. M.: Evidence for enhanced mixing over rough topography in the abyssal ocean, Nature, 403, 179–182, https://doi.org/10.1038/35003164, 2000.

Lee, S., Lumpkin, R., Baringer, M. O., Meinen, C. S., Goes, M., Dong, S., Lopez, H., and Yeager, S. G.: Global Meridional Overturning Circulation Inferred From a Data-Constrained Ocean & Sea-Ice Model, Geophysical Research Letters, 46, 1521–1530, https://doi.org/10.1029/2018GL080940, 2019.

Lee, S.-K., Lumpkin, R., Gomez, F., Yeager, S., Lopez, H., Takglis, F., Dong, S., Aguiar, W., Kim, D., and Baringer, M.: Human-induced changes in the global meridional overturning circulation are emerging from the Southern Ocean, Commun Earth Environ, 4, 69, https://doi.org/10.1038/s43247-023-00727-3, 2023.

Lellouche, J.-M., Greiner, E., Le Galloudec, O., Garric, G., Regnier, C., Drevillon, M., Benkiran, M., Testut, C.-E., Bourdalle-Badie, R., Gasparin, F., Hernandez, O., Levier, B., Drillet, Y., Remy, E., and Le Traon, P.-Y.: Recent updates to the Copernicus Marine Service global ocean monitoring and forecasting real-time 1⁄12° high-resolution system, Ocean Sci., 14, 1093–1126, https://doi.org/10.5194/os-14-1093-2018, 2018.

Li, Q., England, M. H., Hogg, A. McC., Rintoul, S. R., and Morrison, A. K.: Abyssal ocean overturning slowdown and warming driven by Antarctic meltwater, Nature, 615, 841–847, https://doi.org/10.1038/s41586-023-05762-w, 2023.

https://doi.org/10.5194/egusphere-2026-3511
Preprint. Discussion started: 29 June 2026

Liang, X., Spall, M., and Wunsch, C.: Global Ocean Vertical Velocity From a Dynamically Consistent Ocean State Estimate, JGR Oceans, 122, 8208–8224, https://doi.org/10.1002/2017JC012985, 2017.

Liu, M. and Tanhua, T.: Water masses in the Atlantic Ocean: water mass ages and ventilation, EGUsphere [preprint], https://doi.org/10.5194/egusphere-2024-1362, 2024.

Lumpkin, R. and Speer, K.: Global Ocean Meridional Overturning, Journal of Physical Oceanography, 37, 2550–2562, https://doi.org/10.1175/JPO3130.1, 2007.

Marshall, J. and Speer, K.: Closure of the meridional overturning circulation through Southern Ocean upwelling, Nature Geosci, 5, 171–180, https://doi.org/10.1038/ngeo1391, 2012.

Marshall, J., Jamous, D., and Nilsson, J.: Reconciling thermodynamic and dynamic methods of computation of water-mass transformation rates, Deep Sea Research Part I: Oceanographic Research Papers, 46, 545–572, https://doi.org/10.1016/S0967-0637(98)00082-X, 1999.

McDougall, T. J. and Ferrari, R.: Abyssal Upwelling and Downwelling Driven by Near-Boundary Mixing, Journal of Physical Oceanography, 47, 261–283, https://doi.org/10.1175/JPO-D-16-0082.1, 2017.

Morrison, A. K., Waugh, D. W., Hogg, A. McC., Jones, D. C., and Abernathey, R. P.: Ventilation of the Southern Ocean Pycnocline, Annu. Rev. Mar. Sci., 14, 405–430, https://doi.org/10.1146/annurev-marine-010419-011012, 2022.

Munk, W. H.: Abyssal recipes, Deep Sea Research and Oceanographic Abstracts, 13, 707–730, https://doi.org/10.1016/0011-7471(66)90602-4, 1966.

Nikurashin, M. and Ferrari, R.: Overturning circulation driven by breaking internal waves in the deep ocean, Geophysical Research Letters, 40, 3133–3137, https://doi.org/10.1002/grl.50542, 2013.

Oka, A. and Niwa, Y.: Pacific deep circulation and ventilation controlled by tidal mixing away from the sea bottom, Nat Commun, 4, 2419, https://doi.org/10.1038/ncomms3419, 2013.

Orsi, A. H., Johnson, G. C., and Bullister, J. L.: Circulation, mixing, and production of Antarctic Bottom Water, Progress in Oceanography, 43, 55–109, https://doi.org/10.1016/S0079-6611(99)00004-X, 1999.

Purkey, S. G., Smethie, W. M., Gebbie, G., Gordon, A. L., Sonnerup, R. E., Warner, M. J., and Bullister, J. L.: A Synoptic View of the Ventilation and Circulation of Antarctic Bottom Water from Chlorofluorocarbons and Natural Tracers, Annu. Rev. Mar. Sci., 10, 503–527, https://doi.org/10.1146/annurev-marine-121916-063414, 2018.

Ruan, X. and Ferrari, R.: Diagnosing Diapycnal Mixing from Passive Tracers, Journal of Physical Oceanography, 51, 757–767, https://doi.org/10.1175/JPO-D-20-0194.1, 2021.

Shah, S. H. A. M., Primeau, F. W., Deleersnijder, E., and Heemink, A. W.: Tracing the Ventilation Pathways of the Deep North Pacific Ocean Using Lagrangian Particles and Eulerian Tracers, Journal of Physical Oceanography, 47, 1261–1280, https://doi.org/10.1175/JPO-D-16-0098.1, 2017.

Shimada, K., Kitade, Y., Aoki, S., Mizobata, K., Cheng, L., Takahashi, K. T., Makabe, R., Kanda, J., and Odate, T.: Shoaling of abyssal ventilation in the Eastern Indian Sector of the Southern Ocean, Commun Earth Environ, 3, 120, https://doi.org/10.1038/s43247-022-00445-2, 2022.

https://doi.org/10.5194/egusphere-2026-3511
Preprint. Discussion started: 29 June 2026

Stommel, H. and Arons, A. B.: On the abyssal circulation of the world ocean — II. An idealized model of the circulation pattern and amplitude in oceanic basins, Deep Sea Research (1953), 6, 217–233, https://doi.org/10.1016/0146-6313(59)90075-9, 1959.

Talley, L.: Closure of the Global Overturning Circulation Through the Indian, Pacific, and Southern Oceans: Schematics and Transports, oceanog, 26, 80–97, https://doi.org/10.5670/oceanog.2013.07, 2013.

Tamsitt, V., Drake, H. F., Morrison, A. K., Talley, L. D., Dufour, C. O., Gray, A. R., Griffies, S. M., Mazloff, M. R., Sarmiento, J. L., Wang, J., and Weijer, W.: Spiraling pathways of global deep waters to the surface of the Southern Ocean, Nat Commun, 8, 172, https://doi.org/10.1038/s41467-017-00197-0, 2017.

Verezemskaya, P., Barnier, B., Gulev, S. K., Gladyshev, S., Molines, J., Gladyshev, V., Lellouche, J., and Gavrikov, A.: Assessing Eddying (1/12°) Ocean Reanalysis GLORYS12 Using the 14-yr Instrumental Record From 59.5°N Section in the Atlantic, JGR Oceans, 126, e2020JC016317, https://doi.org/10.1029/2020JC016317, 2021.

Waterhouse, A. F., MacKinnon, J. A., Nash, J. D., Alford, M. H., Kunze, E., Simmons, H. L., Polzin, K. L., St. Laurent, L. C., Sun, O. M., Pinkel, R., Talley, L. D., Whalen, C. B., Huussen, T. N., Carter, G. S., Fer, I., Waterman, S., Naveira Garabato, A. C., Sanford, T. B., and Lee, C. M.: Global Patterns of Diapycnal Mixing from Measurements of the Turbulent Dissipation Rate, Journal of Physical Oceanography, 44, 1854–1872, https://doi.org/10.1175/JPO-D-13-0104.1, 2014.

Waugh, D. W., Hall, T. M., and Haine, T. W. N.: Relationships among tracer ages, J. Geophys. Res., 108, 2002JC001325, https://doi.org/10.1029/2002JC001325, 2003.

Wynne-Cattanach, B. L., Couto, N., Drake, H. F., Ferrari, R., Le Boyer, A., Mercier, H., Messias, M.-J., Ruan, X., Spingys, C. P., Van Haren, H., Voet, G., Polzin, K., Naveira Garabato, A. C., and Alford, M. H.: Observations of diapycnal upwelling within a sloping submarine canyon, Nature, 630, 884–890, https://doi.org/10.1038/s41586-024-07411-2, 2024.